Transactions of the SMiRT 27
Yokohama, Japan, March 3-8, 2024
Division X

A METHOD FOR FRACTURE TOUGHNESS PREDICTION OF PRE-STRAINED MATERIALS

Ki-Wan Seo[1], Yun-Jae Kim[2]

[1] Ph. D student, Korea University, Republic of Korea, Seoul, Korea (ayzlayzlzl@korea.ac.kr)
[2] Professor, Korea University, Republic of Korea, Seoul, Korea (kimy0308@korea.ac.kr)

INTRODUCTION

Embrittlement of material occurs due to many reasons: thermal embrittlement, irradiation embrittlement, and hydrogen embrittlement. Typical embrittlement decreases the ductility and fracture toughness of materials. The embrittled material can be experimentally evaluated but the preparation of test specimens was limited, especially irradiation-embrittled materials. Some researchers found that the stress-strain behaviours and fracture toughness of irradiation-embrittled material showed similar results to that of cold-worked material (Jitsukawa et al., 1991, Jitsukawa et al., 1996). The effect of pre-strain due to cold-work on stress-strain behaviours and fracture toughness has been studied in many works (Lie et al., 2018, Thuillier et al., 2018), but the numerical method to quantify the pre-strain effect on ductile fracture simulation was yet clear. In this study, the methodology for quantification of the pre-strain effect on ductile fracture using the multi-axial fracture strain damage model is proposed and validated using experimental fracture toughness tests using cold-worked stainless steel 316.

SUMMARY OF EXPERIMENTS

The published tensile and fracture toughness test using stainless steel 316 (SUS316) was used in this study (Kamaya et al., 2015). Both specimens were extracted from the cold-worked plate. The original thickness of 45 mm was decreased by as much as 20 % after cold-work. Tensile and fracture toughness tests were conducted using the specimen with 0 % to 20 % cold-work, but fracture toughness test with 0% cold work could not provide the valid data. Test cases are summarized in Table 1.

Table 1. Summary of test cases (Kamaya et al., 2015).

Material	Test	Cold-work [%]
SUS316	Smooth Round Bar tensile test, SRB	0, 5, 10, 20
	Compact Tension test, C(T)	5, 10, 20

TENSILE TEST ANALYSIS OF PRE-STRAINED SUS316

The pre-strained specimens were typically prepared using the following two different methods:
(1) Method 1: Pre-strain is applied to a small specimen with loading and unloading procedure (Fig. 1(a))
(2) Method 2: A specimen was extracted from a pre-strained large plate block (by cold-work).
Note that the pre-strain does not change tensile strength when a specimen was prepared using the method (1): tensile strength remains the same for all pre-strain materials. On the other hand, pre-strain increases tensile strength when the specimen is prepared using the method (2). Such inconsistent results come from the definition of a cross-sectional area for the calculation of engineering stress.

For both methods 1 and 2, the engineering stress was calculated using the sectional area A_0 (see Fig. 1(a) and 1(b)). The difference is that A_0 denotes the initial area before pre-straining in the method 1, but the area after pre-straining (thus smaller) in the method 2. Consequently, the engineering stress in the method 2 should be higher than that in the method 1. As results, the tensile

strength in the method 2 can increase with pre-strain due to the smaller cross-sectional area. If the initial area before pre-straining is used during the test by method 2, the engineering stress from the test can be corrected using

$$S_{corr} = S \cdot \frac{(S_u)_{PS=0}}{(S_u)_{PS}} \tag{1}$$

where S_{corr} and S denotes the corrected and original engineering stress, respectively; S_u denotes tensile strength and the subscript, PS=0 and PS, indicates the material properties for un-strained and pre-strained material, respectively.

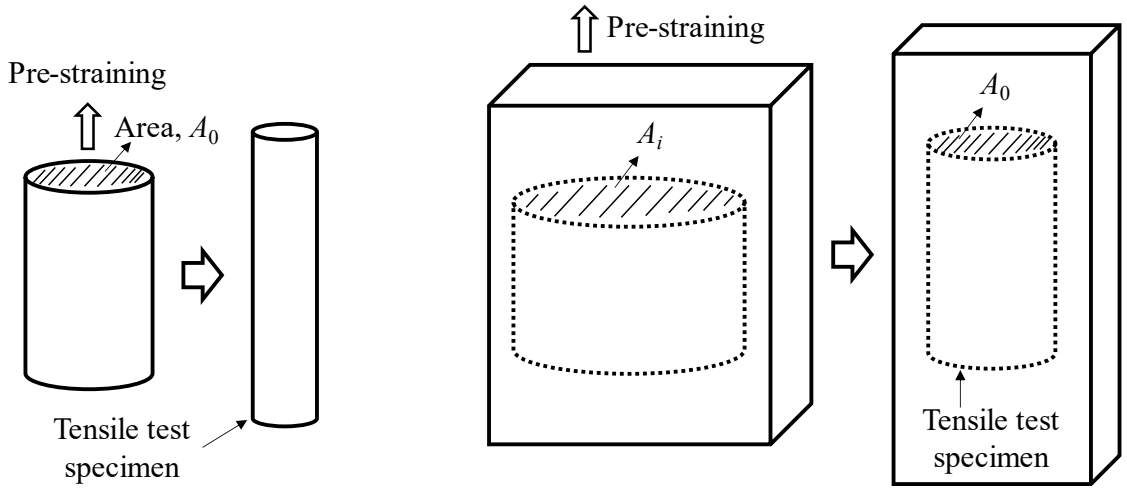

Figure 1. Fabrication of the pre-strained specimen and the definition of the cross-sectional area: (a) method 1 and (b) method 2.

The un-corrected engineering stress-strain curve (raw data in the paper by Kamaya et al., 2015) and corrected stress-strain curve using Eq. (1) are shown in Fig. 2(a) and 2(b), respectively. The relationship between pre-strain ε_{PS} and cold-work was determined as the value by matching the corrected curve for pre-strained material to that for no pre-strained material as shown in Fig. 3(a). The resulting variation of pre-strain with cold-work is shown in Fig. 3(d), showing that the pre-strain is slightly different from the value of cold-work.

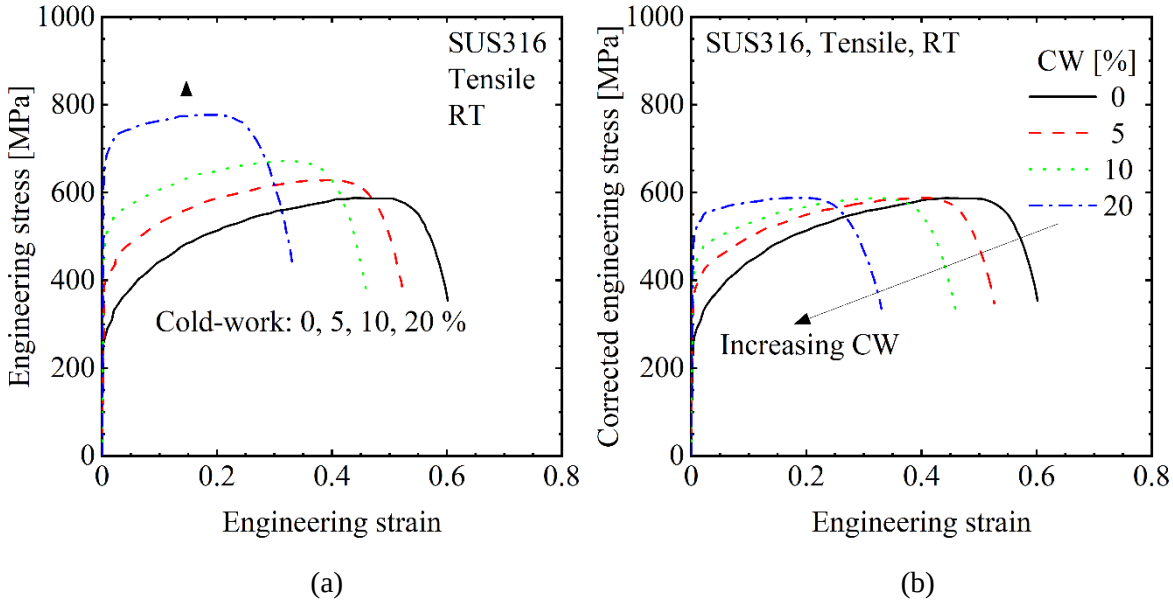

Figure 2. Engineering stress-strain curve of SUS316: (a) un-corrected curves (Kamaya et al., 2015) and (b) corrected curves.

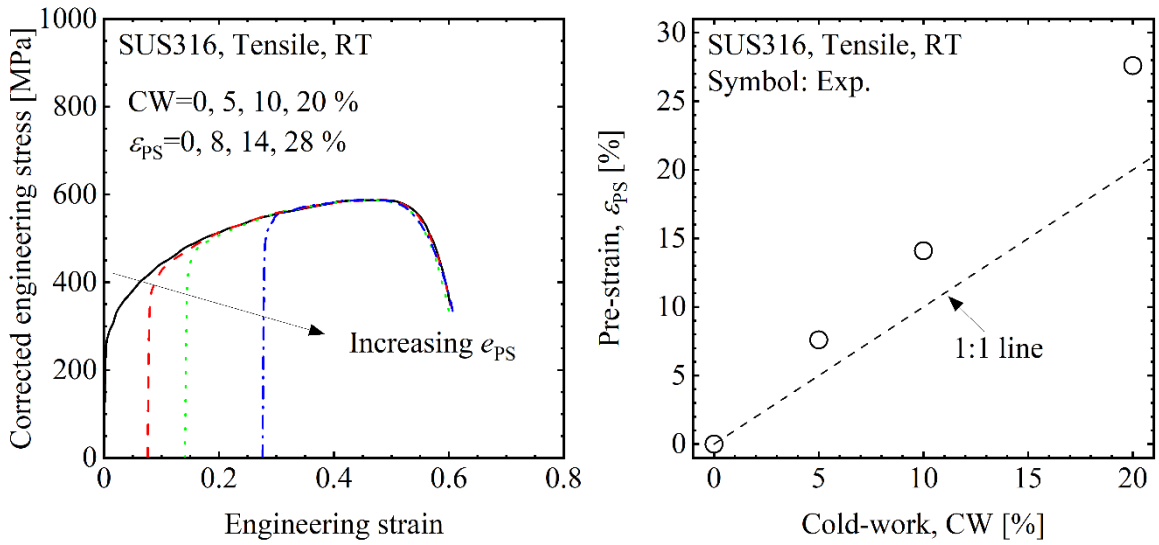

(a) (b)

Figure 3. (a) determination of pre-strain by shifting corrected engineering stress-strain curve and (b) the variation of determined pre-strain with cold work.

ESTIMATION OF TRUE STRESS-STRAIN CURVE FOR PRE-STRAINED SUS316

The true stress-plastic strain curve for pre-strained material can be estimated by shifting the curve of un-strained material by the amount of pre-strain ε_{PS} (Liu et al., 2018). In this study, the true stress-plastic strain curve for pre-strained SUS316 was estimated based on the result and such estimation procedure was validated by simulating the tensile test results in Fig. 2(a). The true stress-plastic strain curve was calculated using engineering stress-strain curve up to necking point. After the necking point, the true curve was determined using both FE analysis and experimental data as proposed by Kamaya et al. (Kamaya and Kawakubo, 2011). The amount of pre-strain in terms of cold-work was determined in Fig. 3(b). It is noted that the SUS316 with 5 % cold-work was assumed as the un-strained material, because the fracture toughness test for 0 % cold-work was not reported (Kamaya et al., 2015).

Figure 4(a) shows the half axis-symmetric FE mesh for tensile simulation, having 955 axis-symmetric second-order elements with reduced integrations (CAX8R) with 0.1 mm element size in the central section. Figure 4(b) shows the estimated true stress-plastic strain curve based on the curve of 5 % cold-worked SUS316. The tensile simulation results, using the FE mesh in Fig. 4(a) and the true stress-plastic strain in Fig. 4(b), are shown in Fig. 4(c), showing good agreement with experimental data.

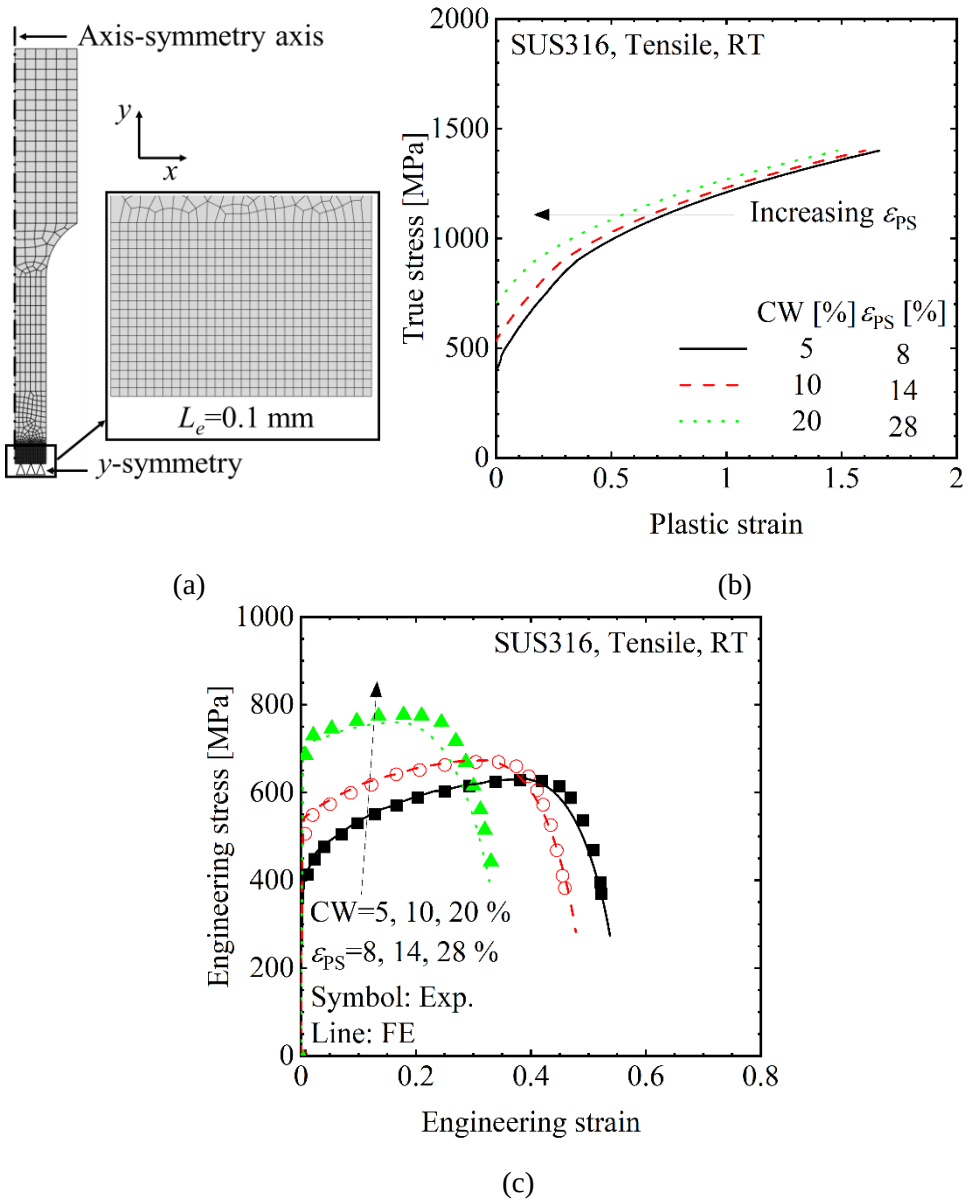

Figure 4. (a) FE mesh for tensile test simulation, (b) estimated plastic strain-true stress curves for pre-strained SUS316 and (c) comparison of simulated engineering stress-strain curve with experimental data.

MULTI-AXIAL FRACTURE STRAIN DAMAGE MODEL

The ductile fracture of pre-strained materials is simulated using multi-axial fracture strain damage model (Seo et al., 2023). In the model, the plastic damage D due to plastic strain ε_p is calculated as follows:

$$D = \int \Delta D;\ \Delta D = \frac{\Delta \varepsilon_p}{\varepsilon_f} \tag{2}$$

where ε_f denotes the multi-axial fracture strain expressed as follows:

$$\varepsilon_f = \alpha \cdot \exp\left(-1.5\frac{\sigma_m}{\sigma_e}\right) + \beta \tag{3}$$

where σ_m and σ_e denotes hydrostatic stress and von-Mises equivalent stress, respectively; α and β are material constants. It is assumed that the ductile fracture occurred when accumulated damage D reaches the critical damage value D_c. In the FE simulation, the effective stress and elastic modulus

were reduced to small values (100 and 20 MPa) when the material failed, and an element that all integration points in the failed element was removed during simulation.

The damage model for pre-strained SUS316 was estimated based on the model for un-strained material. The damage model for un-strained material was determined using tensile and fracture toughness tests. Firstly, the tensile test was simulated and the variation of stress-triaxiality with plastic strain up to failure was calculated at the center point as shown using a solid line in Fig. 7(a). The averaged stress-triaxiality with plastic strain gives one point in the fracture strain locus as shown using a square symbol in Fig. 7(b). Secondly, the parameters in Eq. (3) were determined by analysis of the fracture toughness test. Typical fracture toughness test gives two distinct properties: crack initiation and crack growth resistance. The critical damage value was determined by simulating the crack initiation and the final values for α and β were determined by simulating the crack growth resistance (J-resistance curve). The detailed procedure can be found in our previous works (Park et al., 2021). The determined fracture strain locus and critical damage value of 1.5 for SUS316 at CW= 5 % are

$$\varepsilon_f = 3.757 \cdot \exp\left(-1.5\frac{\sigma_m}{\sigma_e}\right) \tag{4}$$

The multi-axial fracture strain model was validated by simulating the fracture toughness test for SUS316 at CW=5 %. Figure 5(a) shows the three-dimensional quarter FE mesh for C(T) simulation consisting of 35,670 eight-node brick elements with full integration (C3D8). The minimal element size at the crack propagation area was set to be 0.2 mm. Fig. 5(b) compared the simulated J-resistance curve with experimental data. It is noted that the simulation was performed with fracture strain locus in Eq. (4) and D_c =1.4, 1.5 and 1.6 to see the effect of D_c on the J-resistance. The J-resistance curve increased with increasing D_c and the simulation result with D_c=1.5 gives good estimation of experimental J-resistance curve.

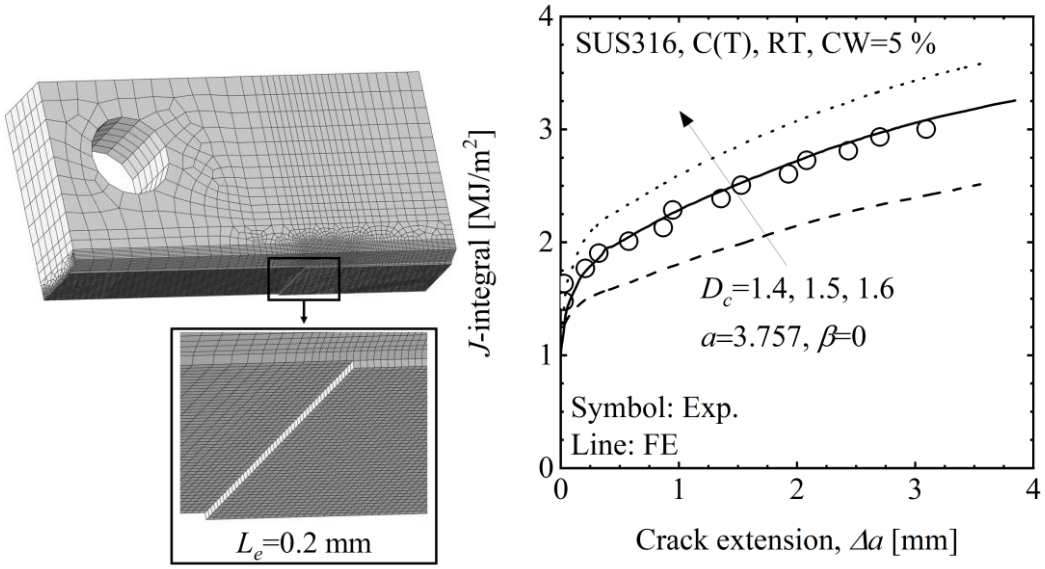

Figure 5. (a) Three-dimensional FE mesh for C(T) simulation and (b) the effect of D_c on simulated J-resistance curve and comparison with experimental data for C(T) test.

ESTIMATION OF DAMAGE MODEL OF PRE-STRAINED SUS316

In this section, the effect of pre-strain on the fracture strain locus and D_c was analysed. The effect of pre-strain on D_c was analysed first. Peng et al. (Peng et al., 2018) proposed energy dissipation variable to quantify a pre-damage due to pre-strain as follows.

$$D_u = 1 - \frac{U_{\mathrm{FED,PS}}}{U_{\mathrm{FED,PS=0}}} = 1 - \frac{\int_{\varepsilon \mathrm{PS}}^{e_u} sde}{\int_0^{e_u} sde} \tag{5}$$

where subscript, PS=0 and PS, represents the property for un-strained and pre-strained material, respectively; s and e denote engineering stress and strain, respectively; e_u denotes the uniform strain; and $\varepsilon_{\mathrm{PS}}$ denotes the amount of pre-strain determined in Fig. 3(b). The parameter U_{FED} represents the fracture energy density (the area under the engineering stress-strain curve up to tensile strength). The second term in right-hand side of Eq. (5) can be regarded as the damage due to pre-strain, D_{PS}

$$D_{\mathrm{PS}} = \frac{U_{\mathrm{FED,PS}}}{U_{\mathrm{FED,PS=0}}} = \frac{\int_{\varepsilon \mathrm{PS}}^{e_u} sde}{\int_0^{e_u} sde} \tag{6}$$

It is noted that the critical damage value of multi-axial fracture strain damage model is represented as D_c, and the ductile fracture is assumed to occur when the accumulated damage reaches critical damage value D_c. The effect of pre-strain on ductile fracture was quantified using D_c and the critical damage value for pre-strained material, $D_{c,\mathrm{PS}}$, can be then estimated from that for the reference (un-strained) material, $D_{c,\mathrm{PS=0}}$:

$$D_{c,\mathrm{PS}} = D_{c,\mathrm{PS=0}} \cdot \frac{U_{\mathrm{FED,PS}}}{U_{\mathrm{FED,PS=0}}} \tag{7}$$

Figure 6(a) shows the variation of U_{FED} with pre-strain. It is noted that the engineering stress-strain curve for pre-strained SUS316 can be simply estimated by shifting the engineering stress-strain curve for un-strained material. The U_{FED} decreased linearly with increasing pre-strain, resulting the linearly decreasing D_c with pre-strain as shown in Fig. 6(b).

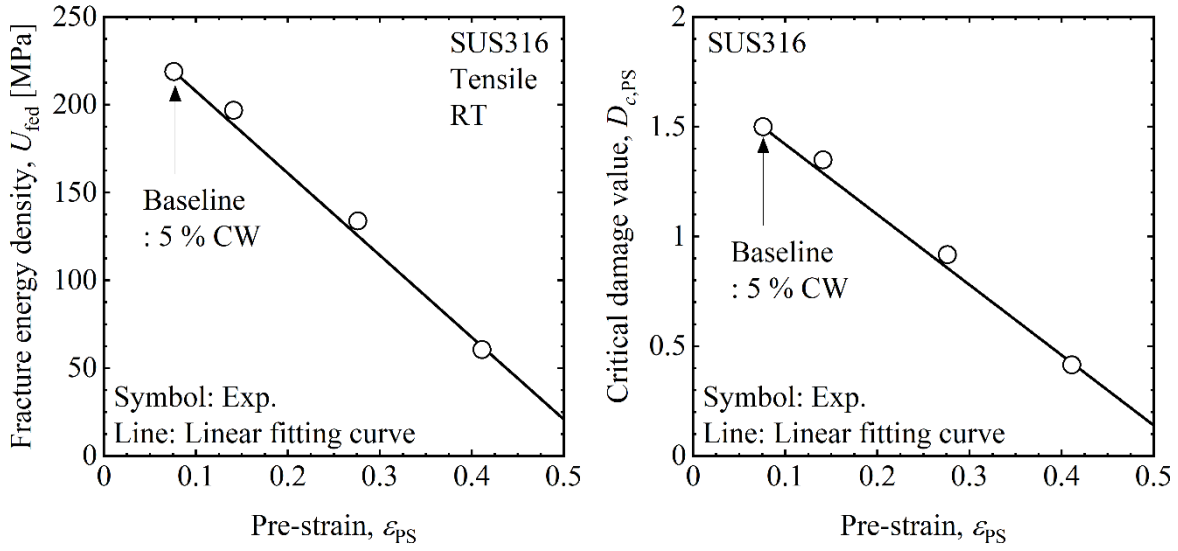

Figure 6. Variations of (a) the fracture energy density U_{FED} and (b) the critical damage value D_c with pre-strain for SUS316.

Secondly, the effect of pre-strain on fracture strain locus was analysed using tensile test of pre-strained SUS316. Note that the fracture strain locus was determined by calculating average stress triaxiality up to fracture at the center point of tensile simulation. Figure 7(a) shows the variation of stress-triaxiality with plastic strain up to failure for pre-strained SUS316. The tensile simulation results for pre-strained SUS316 can be shown in Fig. 4(c). The variation of fracture strain with averaged stress-triaxiality was shown in Fig. 7(b). The fracture strain decreased, however, the averaged stress-triaxiality increased with increasing pre-strain. The averaged points remain on the fracture locus for un-strained material as shown in Fig. 7(b). Because the SUS316 has very large

fracture strain (1.67), the effect of pre-strain on the fracture strain was not significant. Consequently, it is assumed that the fracture strain locus is not affected by pre-strain.

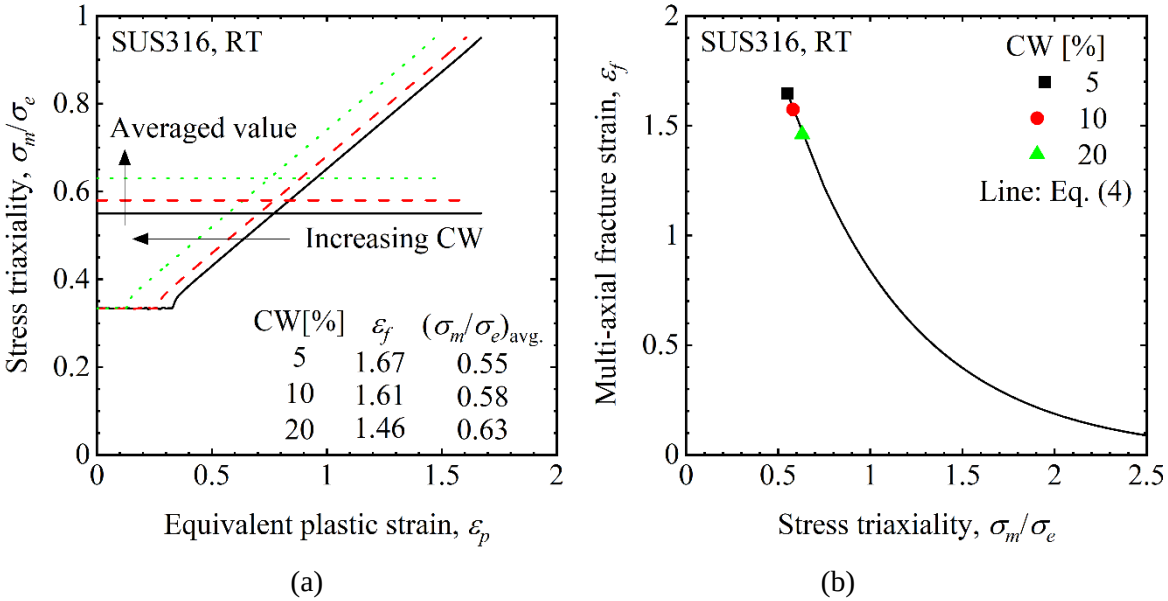

(a) (b)

Figure 7. (a) Variation of stress triaxiality with plastic strain and (b) fracture strain locus.

VALIDATION OF PROPOSED FRACTURE TOUGHNESS PREDICTION METHOD USING EXPERIMENTAL DATA

The estimated multi-axial fracture strain damage model for pre-strained SUS316 is validated by simulating the fracture toughness test for pre-strained SUS316 in this section. FE damage analyses were performed using the estimated damage model. The FE model in Fig. 5(a) was used with the damage model for pre-strained material: true stress-plastic strain curve in Fig. 4(b) and critical damage value in Fig. 6(b). Figure 8 compares the simulated *J*-resistance curve with experimental data, showing good agreement.

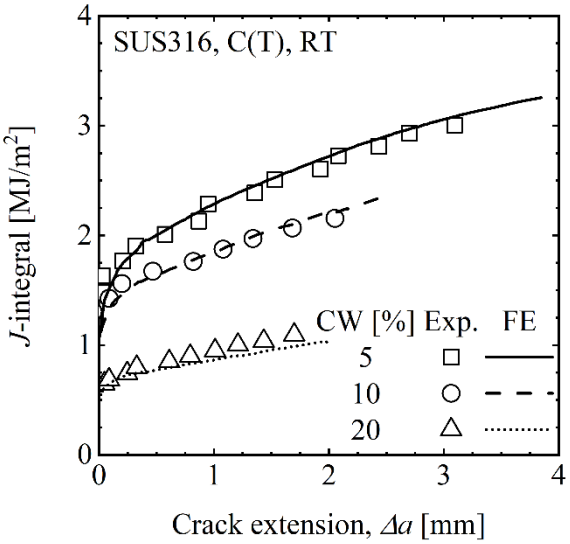

Figure 8. Comparison of simulated *J*-resistance curve with the experimental data of pre-strained SUS316.

CONCLUSION

In this study, the pre-strained SUS316 was analysed and the method to estimate the fracture toughness of pre-strained SUS316 was proposed. The estimation of true stress-plastic strain for pre-strained SUS316 was performed by shifting the curve for un-strained material by the amount of pre-strain. The critical damage value of pre-strained material was estimated using the fracture energy density ratio of pre-strained material to un-strained material and the fracture locus was assumed to be constant independently with the pre-strain. The proposed method was validated by simulating the fracture toughness test for pre-strained SUS316. The estimated *J*-resistance curve was compared with the experimental data, showing good agreement.

REFERENCES

Jitsukawa S, Shiba K, Hishinuma A, Alexander DJ, Pawel JE. "Comparison of elastic—plastic fracture toughness of irradiated and cold-worked JPCA using miniaturized DCT specimens". *J Nucl Mater* 1996;233–237:152–5.

Jitsukawa S, Grossbeck ML, Hishinuma A. "Stress-strain relations of HFIR-irradiated austenitic stainless steels". *J Nucl Mater* 1991;179–181:563–7.

Liu B, Villavicencio R, Guedes Soares C. Experimental and numerical analysis of residual stresses and strains induced during cold bending of thick steel plates. *Mar Struct* 2018;57:121–32.

Thuillier S, Zang S-L, Troufflard J, Manach P-Y, Jegat A. Modeling Bake Hardening Effects in Steel Sheets—Application to Dent Resistance. *Metals* (Basel) 2018;8:594.

Kamaya M. Elastic-plastic failure assessment of cold worked stainless steel pipes. *Int J Press Vessel Pip* 2015;131:45–51.

Kamaya M, Kawakubo M. A procedure for determining the true stress-strain curve over a large range of strains using digital image correlation and finite element analysis. *Mech Mater* 2011;02:007.

Park EK, Youn GG, Kim YJ, Ainsworth RA. The effect of material ductility on notch fracture resistance: Numerical study. *Theor Appl Fract Mech* 2021;112:102874.

Seo K-W, Kim Y-J, Hwang J-H, Kim K-S. Finite element simulation method for combined Ductile-Brittle fracture of small punch test in hydrogen. *Eng Fract Mech* 2023;289:109489.